Properties of a-(Si,Ge) films and devices deposited at high growth rates

by

Caustoobh Kashyap Bezboruah

A thesis submitted to the graduate faculty

in partial fulfillment of the requirements for the degree of

MASTER OF SCIENCE

Major: Electrical Engineering

Major Professor: Dr. Vikram L. Dalal

Iowa State University

Ames, Iowa

2000

Graduate College

Iowa State University

This is to certify that the Master's thesis of

Caustoobh Kashyap Bezboruah

has met the thesis requirements of Iowa State University

Signatures have been redacted for privacy

to

ma-deeta,

my parents-

one of you will not

get to see this...

~~

TABLE OF CONTENTS

ABSTRACT

In this thesis, we study the properties of amorphous silicon germanium thin films and devices deposited at high growth rates. The effect on the optical and electrical properties of amorphous silicon germanium samples is reported. The films and devices are prepared by ECR-CVD from silane and germane feed gases. Helium plasma is used to obtain faster growth rates of the films. The report records the thin films quality in terms of the optical gaps - E04 and Tauc gaps, photo and dark conductivities, sub-gap absorptions and Urbach energies, and activation energies. Based on these observations, good quality p-i-n solar cells have been fabricated.

Undoped amorphous silicon germanium films were deposited on 7059 corning glass with growth rates of 4.5-5 A/sec. The microwave power was at 150W and the silane flow was at 3sccm. The effect of the substrate temperature, chamber pressures and germane flow were studied.

We used the optimum deposition parameters obtained from the growth of films for the p-i-n devices. We varied the graded ppm boron doping of the i-layer, and the deposition times, and hence the thicknesses of the SiC buffer layer between the p and i-layers. We report good device characteristics with open-circuit voltage of 0.69 V , fill factor of 67% ,and good QE properties for SiGe devices with a Tauc gap of 1.6 eV .

1. INTRODUCTION

Hydrogenated amorphous silicon (a-Si:H) has spawned a rapidly developing amorphous semiconductor industry as it is unmatched as the switching material in large area liquid crystal displays, as a photoreceptor for photovoltaic panels and solar cells, optical memories and any other application that needs a high quality semiconductor that can be processed on large, curved or flexible substrates. The subject was brought to the attention of the scientific and business community in 1968 by S. R. Ovshinsky, who advocated the use of chalcogenide materials for electronic switching. The present impetus has resulted from breakthroughs in thin film amorphous silicon alloy films made by W. E. Spear's group at the University of Dundee in Scotland, which led to the demonstration of viable solar cell devices by D. E. Carlson and C. R. Wronski of the RCA laboratories [1].

This introduction outlines the novel features of a-Si:H. A complete description of the physics of amorphous semiconductors can be found in Madan and Shaw [2], and Street [3].

Hydrogenated amorphous silicon germanium (a-SiGe:H) alloy thin films have tremendous potential as a material for optoelectronic applications. The first a-SiGe:H alloys were fabricated by Chevallier et al [4] in 1977 using RF plasma enhanced chemical vapor deposition (PECVD) from a silane and germane gas mixture. The main advantage of the material is the tunability of its optical bandgap to match with the lower energy portion of the solar spectrum (1.0-1.7 eV) by controlling the germanium content in the material [4]. This makes the material a good candidate for meeting the requirements of, e.g., stacked solar cells and optoelectronic devices where a certain bandgap, a variety of different bandgaps or other material properties are needed. Proper exploitation of this material can increase the efficiency and stability of a multijunction a-Si solar cell. Si-based thin film solar cells including a-SiGe:H layers have the highest stable efficiency of 13% [5]. Other applications like multispectral colour sensors have also been developed [6].

However, the properties of a-SiGe:H even at best have remained inferior to high quality a-Si:H. This is because with alloying and the required shift of the optical gap, other material properties are also influenced in a way detrimental to technical applications. The sub-gap defect densities and Urbach energies for tail states are higher in a-SiGe:H. It is believed that one of the reasons for inferior properties is the lower surface mobility during growth of the germyl radical as compared to the silyl radical. This causes a high density of voids or clustered Ge-Ge bonds in the material. Researchers have therefore concentrated on the investigation of the growth process, and proposing and testing alternative deposition techniques in order to control the material properties.

This report presents the results of controlled ion bombardment from a He plasma, generated by an Electron Cyclotron Resonance (ECR) plasma reactor to improve the material properties of a-SiGe:H alloys.

The advantages of ECR-CVD over conventional glow discharge include
(a) efficient energy transfer from the microwave field to the plasma;
(b) control of ion energy by the gas pressure;
(c) high utilization of feedstock gases;
(d) lower operating pressures;
(e) better control of the dissociation of the deposition gas;
(f) high ion densities;
among others.

Plasma deposition has the added advantage of being a product of simultaneous etching and deposition. It is believed the etching process during growth preferentially removes the weaker bonds leading to a better network.

The understanding of the deposition processes of a-SiGe:H is rather inconclusive. Doyle et al [8] have reported a detailed study of the plasma chemistry in silane/germane and disalane/germane mixtures. Dalal et al [9] have also investigated the growth chemistry of these alloys.

Several seemingly partly contradictory optimum growth conditions have been suggested which include, among others:

a) reducing short lifetime radicals through reaction with H_2 or avoiding depletion of germane [10];
b) enhancing surface diffusion of Ge related radicals by hydrogen coverage [11];
c) using an alternative Ge dangling bond terminator [12];
d) needing no [13], versus high energy ion bombardment (or high ion bombardment at high deposition rate [14]) to reduce heterogeneities and obtain optimum performance [9,15-16]
e) using higher electron temperatures for the PECVD process to obtain a favourable discharge chemistry [16];
f) needing low [17,18] versus high [19,20,21] deposition rates.

Hydrogen dilution was first reported by Matsuda et al in 1986 [11] in order to improve material properties. The hydrogen dilution method was quite successful in improving electronic properties at a given optical gap. Some results from hydrogen dilution of process gases are given in [14,16,17,22-24].

Stutzmann et al [25] discuss the properties of a-SiGe:H material with Ar, Ne, He and H_2 dilution. Tsuo et al [26] also compare H_2 , He and Ar dilution and report improved mobility-lifetime product and ambipolar diffusion length with He dilution but unaltered photoconductivity and sensitivity. Middya et al [17] also compare effects of H_2 and He dilution and different deposition rates.

Dalal et al [9] have earlier reported good material properties with ion bombardment in helium plasma with low (1-1.5 A/sec) growth rates.

We have in this case used a He plasma to achieve growth rates of ~ 5 A/sec and report good material and device properties.

The films and devices were prepared in an ECR-CVD reactor using silane and germane in a helium plasma. The objective was to characterize the film properties and to fabricate devices using the optimum parameters. The electrical and optical properties of the films measured include thickness, band gap energies, photo and dark conductivity, sub-bandgap absorption, Urbach energy and activation energy. The device parameters used to characterize them are the I-V characteristic, the quantum efficiency, the Urbach energy and mid-gap states.

2. SAMPLE FABRICATION

2.1 Sample Growth

The samples, both films and devices were fabricated using a remote, low pressure ECR plasma to generate a beam of helium atoms and ions. The samples were grown by Tim Maxson, Kay Han, Vu Anh Vu and Zhiyang Zhou in Dr Dalal's group. The setup for the ECR CVD reactor is shown in Appendix A.

The use of a helium plasma allows higher growth rates. The plasma beam impinges on the sample and reacts with the silane and germane introduced near the substrate to cause growth of the film [27]. The plasma potential and plasma density reaching the substrate are known to be functions of pressure in the reactor and the power density of the incoming microwave beam, which excites the plasma [28].
The films were deposited on 7059 glass substrates and the devices on stainless steel substrates. The substrates were cleaned using a cleaning process consisting of boiling in acetone and methanol solution.

A system cleaning process involving gas purges with nitrogen, silane and argon in vacuum to remove the moisture from the system is done immediately following loading the substrates into the reactor chamber. The substrate is heated to a temperature at least 50 C higher than the deposition temperature to allow out gassing of impurities and moisture from the substrate and the sample itself. A silane-hydrogen cleaning plasma is then used to etch off any remaining impurities from the chamber walls and deposit a pure amorphous silicon coat on the inside surface of the system. The plasma gases are introduced remote from the substrate and ignited by microwaves. During the deposition process, a shutter, placed between the substrate and the plasma, is opened and the films deposited. The dopant gases are introduced into the chamber using a separated manifold, in order to minimize cross contamination between dopant and intrinsic gases.

The devices fabricated are p-i-n solar cells. First, a ~0.5μm phosphorus doped n+ layer is deposited on the stainless steel substrate. Then the intrinsic or i-layer of thickness

~0.4μm is deposited for the desired silane-germane flow rates and deposition conditions. The band gap of this layer may be graded to improve efficiency. This is followed by a thin graded SiC buffer layer to match the band-gaps of the a-SiGe i-layer to the p a-(SiC):H layer. The following boron doped p-layer of a-(SiC):H is of thickness 0.02 - 0.03μm. This minimizes absorption in the p layer as well as provides a good recombination junction [29]. The buffer layer therefore allows for the bandgap to change smoothly from the high gap p layer to the low gap i layer. Dalal et al [29] have explained in detail the design of the grading scheme.

Combinations of indicated substrate temperatures of 300 and 350^{0}C; microwave powers of 150 and 200W; pressures of 15 and 20 mTorr; and three different ratios of GeH_4 and SiH_4 were used. Indicated temperatures are 30 - 40 ^{0}C higher than the actual temperature. Helium is used as the ECR plasma excitation gas in order to achieve growth rates of 4-5 A/sec. The basic properties such as, electrical, optical, and structural properties of the film are strongly dependent on the substrate temperature, microwave power, as well as the gas flow rates during the deposition.

2.2 Contact Metallization

Chromium contacts deposited by thermal evaporation, followed by silver paint on top is used for electrical measurements on films. The thermal evaporator system consists of a bell jar with resistively heated chromium rods. A mask providing a length to width ratio of 20 is used to selectively deposit the metal. The chromium layer of about 1000 A is deposited in a vacuum of 3 μTorr at a rate of 5-7 A/sec. Silver paint is applied on top of the chromium contacts to provide the good contacts to the metal probes. The samples are than annealed at 180^{0}C for at least one hour.

Contacts for devices have a 100 A semi-transparent chromium dot followed by a 1000 A thick aluminum busbar for an ohmic contact.

3. CHARACTERIZATION TECHNIQUES

3.1 Characterization Of Films

To analyze the optical and electrical properties of the thin films prepared by the ECR-CVD system, many measurements have been performed. These measurements include UV/VIS/NIR spectroscopy, photo and dark conductivity, sub-bandgap absorption, activation energy, and Urbach energy. Using the data from these, it is possible to determine the electrical, optical properties, and the quality of thin films.

3.1.1 Thickness Measurement

A Lambda-9 dual beam spectrophotometer is used for investigating the thickness, absorption coefficient and optical bandgap of the a-S:Ge films. The thickness of thin films is determined by the oscillation period of the transmission versus wavelength curve in the 600 to 2000 nm spectrum range as shown in Figure 3.1.

The thin films are grown on top of Corning 7059 glass. As the glass is much thicker compared to the film, it does not contribute to any interference effects, and therefore its effect is neglected.

The film is mounted perpendicular to the light rays. At the surface, the reflected rays undergo a phase change of half of a wavelength. At the thin film-glass interface, the index of refraction of the film being greater than that of the glass, reflection does not cause a phase change. The condition for destructive interference is such that,

$$2t \sin\theta = m\lambda/\eta$$

where t is the thickness of the thin film, λ is the wavelength, η is index of refraction of the film, for $\theta = \pi/2$, $\sin\theta = 1$ and m an integer number. The thickness can be determined by any two adjacent minimas λ_1 and λ_2 and is given by,

$$t = \frac{\lambda_1 \lambda_2}{2\eta(\lambda_1 - \lambda_2)}$$

If we use the peaks from a transmission scan instead of a reflection scan, λ_1 and λ_2 should be the maximas instead of the minimas. The refraction index of the film can be determined by solving for η in the expression:

$$Avg\langle R\rangle = (\frac{\eta - 1}{\eta + 1})^2$$

where Avg<R> is the average reflection in the non-absorbing range (1000 - 2000 nm). The refractive index is assumed constant over the range of wavelength used.

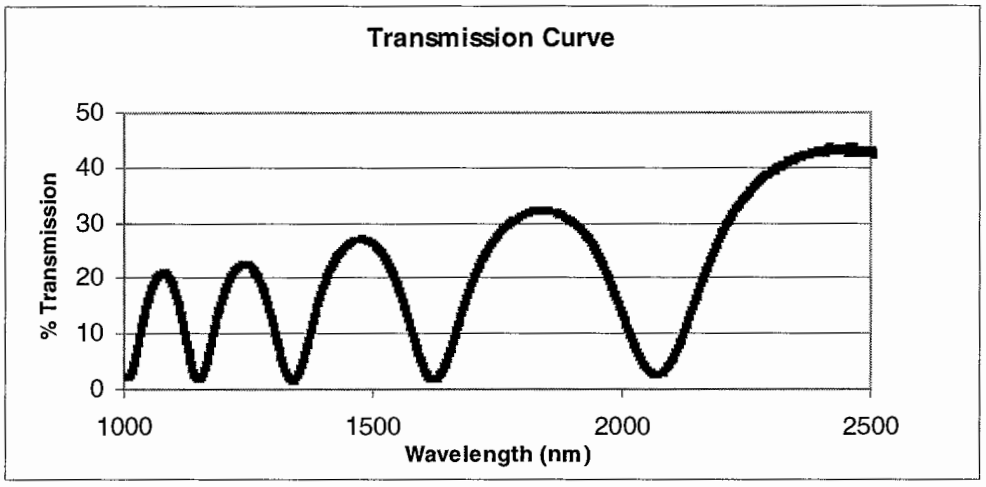

Figure 3.1 Plot showing transmission as a function of wavelength for a typical film

3.1.2 Absorption Coefficient and E_{04}

Measuring the absorption spectrum is the most direct and perhaps the simplest method for probing the band structure of semiconductors. In the absorption process, a photon of a known energy excites an electron from a lower to a higher energy state. Thus, by placing the thin film at the output of a monochromator beam and studying the changes in the transmitted radiation, it is possible to discover all the possible transitions an electron can make and learn much about the distribution of states.

Fundamental absorption refers to band-to-band or exciton transitions, i.e.,

to the excitation of an electron from the valence band to the conduction band. Thus the fundamental adsorption, which manifests itself by a rapid rise in absorption (Figure 3.2), can be used to determine the energy gap of the semiconductor.

The absorption coefficient as a function of wavelength can be calculated using the following expressions for the absorption, reflection, and transmission as the functions of the wavelength of the incident photons

$$A(\lambda) = \log \frac{1}{T(\lambda)}$$

$$T(\lambda) = [(1-R(\lambda)] \exp[-\alpha(\lambda)\, t]$$

where $A(\lambda)$ is the absorption, $T(\lambda)$ is the transmitted light intensity, $R(\lambda)$ is the reflectivity, t is the thickness of the film, and $\alpha(\lambda)$ is the absorption coefficient. The absorption coefficient as a function of the wavelength can be calculated by combining the expression for $A(\lambda)$and $T(\lambda)$ and solving for the value of $\alpha(\lambda)$, which is found to be

$$\alpha(\lambda) = 2.3\ [A - \log_{10}(\ 1/(1-R)\ )]\ /t$$

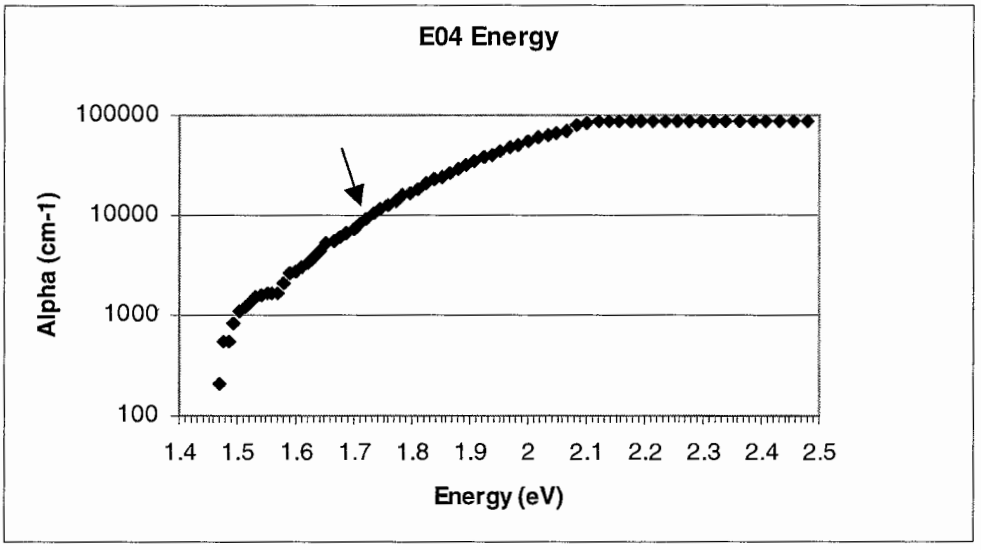

Figure 3.2 Absorption coefficient as a function of photon energy. The arrow points to the E04 energy.

A plot of $\alpha(\lambda)$ versus E_{ph} provides visual information about absorption edge. The energy for which $\alpha(\lambda) = 10^4$ cm^{-1} is denoted as E_{04} energy gap, and is a useful indicator of the optical properties of the material.

3.1.3 Tauc Energy Gap

Tauc [30] used the approach of defining the optical bandgap in terms of extrapolation of the bands to get the empirical relationship

$$\sqrt{\alpha(\lambda)h\nu} = B(h\nu - E_{tauc})$$

where $\alpha(\lambda)$ is the absorption coefficient, h is Planck's constant, ν is the radiation frequency (the radiation energy, $h\nu = 1240/\lambda$ (eV)), and B is a proportionality constant. The E_{Tauc} is determined by extrapolating the linear part of the plot (Figure 3.3) of the square root of the product of the absorption coefficient and photon energy vs photon energy to the photon energy axis, $h\nu$.

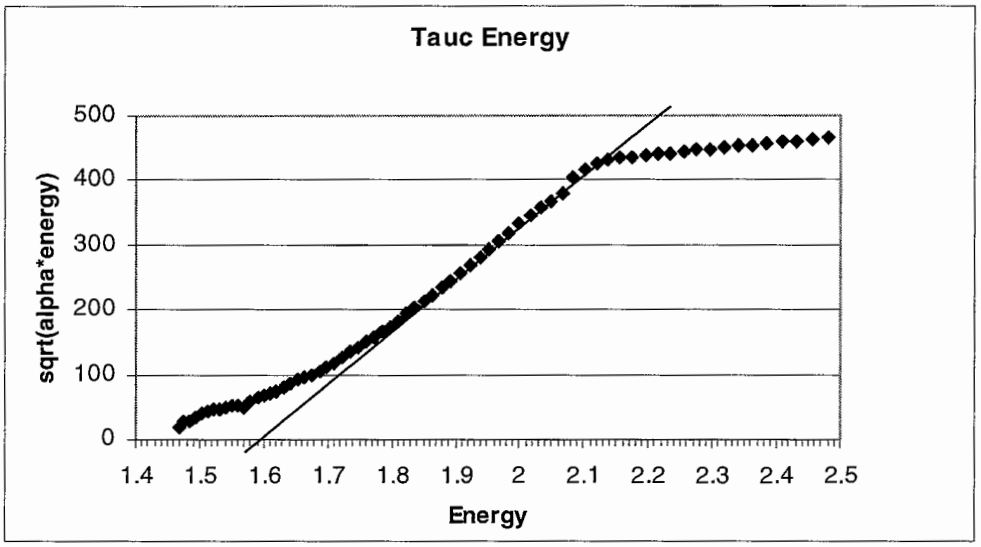

Figure 3.3 Plot for determining the Tauc energy

It is assumed that the density of states distribution increases as a power law of the energy from an extrapolated conduction band edge, with a similar shape for the valence band. It is also assumed that the matrix elements are energy independent and the band edges are parabolic. Though the matrix elements are not exactly constant and the band

edges are more nearly linear than parabolic, these effects cancel out. The mobility gap - defined as the energy separation of the valence and conduction band mobility edges - generally has a larger energy [3].

Intrinsic a-Si has a Tauc gap of 1.7 - 1.8 eV while a-Ge has a Tauc bandgap of about 1.1 eV. Depending on the Ge content in a-Si:Ge, a Tauc bandgap of 1.1 - 1.7 eV can be achieved [4].

3.1.4 Photo And Dark Conductivity

Photoconductivity is the change in the electrical conductivity when a material is exposed to electromagnetic radiation. Since the measurements are important as well as simple, photo and dark conductivities are amongst the first set of properties measured.

An excess conductivity $\Delta\sigma$ given by,

$$\Delta\sigma = e(\Delta n\mu_n + \Delta p\mu_p)$$

appears if, under the action of absorbed light, the densities of the charge carriers n and p increase compared with their values at thermal equilibrium.

Photosensitivity is the ratio of the photo to the dark conductivity. Amorphous materials absorb photons very efficiently and so they have a large photosensitivity. The measurement involves placing the sample on a base and probes being connected to the sample contacts. An ELH lamp biased at 105 V and calibrated to the strength of one sun is used as the light source. The whole apparatus is enclosed in a chamber that prevents any photo generation of charge carriers when light source is off. A fan keeps the sample at room temperature. The conductivity is given by the expression:

$$\sigma_{d,\,ph} = \frac{WI}{LVt}$$

where L/W is the length to width ratio of the metal contacts (which is 20), t is the film thickness, V is applied voltage, and I is the measured current.

3.1.5 Activation Energy

This characterization technique measures the activation energy due to the thermal excitation. Activation energy (Figure 3.4) of an amorphous film can be used to directly determine the Fermi level from the temperature dependence of the conductivity. The expression for the conductivity can be obtained from Fermi statistics as

$$\sigma = \sigma_o \exp(-E_A/kT)$$

with the activation energy given by

$$E_A = E_{c,v} - E_{fn,p}$$

where $E_{c,v}$ is the conduction or valence band edge defined by the mobility gap, $E_{fn,p}$ is the quasi-Fermi level, and σ_o is the conductivity prefactor known as the minimum metallic conductivity and is a constant. The above approximation is true only if the mobility is a weak function of the temperature and if the presence of deep levels does not alter the occupation statistics of band states too severely.

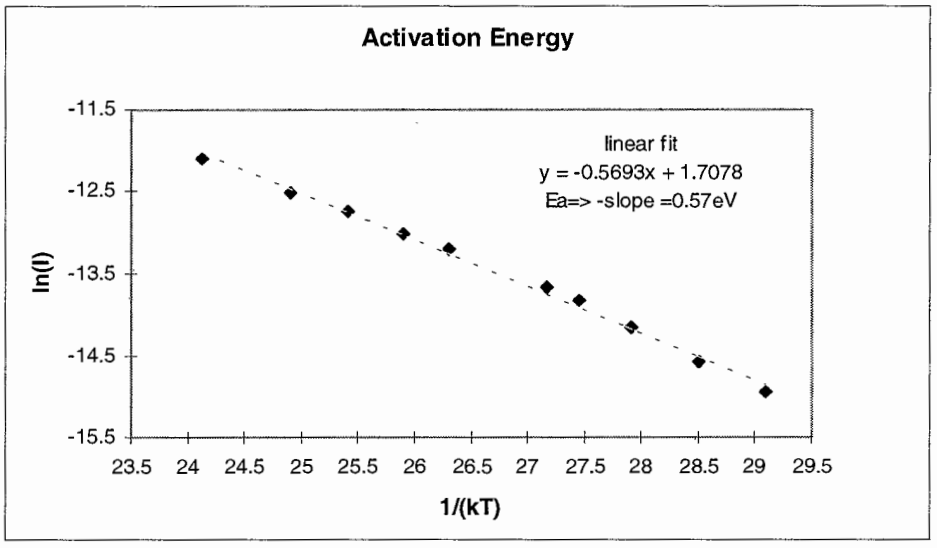

Figure 3.4 Plot of logσ vs T^{-1} for computing the activation energy of the material

The activation energy can be extracted from the Arrhenius plot of the logarithm of the conductivity (or equivalently the current since σ is proportional to the measured current) over a temperature range (80 - 200 °C). The upper limit is kept below 200 °C to limit changes in the band structure. Also, to prevent the photogeneration of charge

carriers, the experiment is performed in a closed, dark environment. The substrate rests on a heater block inside a closed box. To enhance the current, a bias of 100V is applied between the probes. A schematic of the setup is shown in Appendix B.

A linear plot of $\log\sigma$ vs T^{-1} could indicate either band-like conduction beyond a sharp mobility edge or phonon-assisted hopping between nearest-neighbour localized states. Alternatively, a concave upward $\log\sigma$ vs. T^{-1} plot could reflect either the absence of a sharp mobility edge or the predominance of variable range hopping conduction [28].

3.1.6 Sub-gap Absorption and Urbach Energy

Sub-gap absorption measurement is useful to get an idea of the quality of films. This requires the measurement of low α (0.1 to 10cm-1). In thin films, as in the present case, the film geometry limits the accurate determination of α from optical reflection and transmission data to $\alpha \geq 1000$cm-1. Then indirect measurements of spectral absorption like electroabsorption, photothermal deflection spectroscopy (PDS) and constant photocurrent method (CPM) are used.

We us the two-beam photoconductivity sub-bandgap absorption technique developed by Wronski and co-workers [31]. A benefit of the two-beam sub-gap technique is that it enables the determination of absorption coefficients of films grown on non-transparent substrates such as stainless steel, polyamide, and molybdenum-coated polyamide.

The technique utilizes a dc light beam of high intensity to fix the quasi Fermi levels, while an ac light beam of low intensity probes the photoconductivity of the sample. The dc beam continuously creates electron-hole pairs that keep the mid-gap states (traps) filled and the occupancy of the mid-gap states constant. This fixes the lifetime of the photo-generated carriers. The ac beam superimposes on the dc beam and thus modulates the sample photocurrent by creation of additional electron-hole pairs. A lock-in amplifier is used to determine the change in photocurrent, which in turn is related to the absorption coefficient. To enhance the measured signal, a bias of 7 volts is placed across the sample to improve the transport of electron-hole pairs. The absorption coefficient is calculated at each wavelength by dividing the signal by that of a reference

cell and multiplying by the quantum efficiency of the silicon/germanium reference detector.

In the experimental apparatus shown in Appendix C, the source is white light and the monochromator is used to change the wavelength of the incident photons. For SiGe, the range of the wavelengths used is from 600 nm to 1300 nm (or higher). Chopping the output of monochromator at 13.5 Hz creates an ac beam. This frequency produces a square wave and reduces the noise due to ambient light and 60 Hz power lines. High pass optical filters are added at 700 nm and 900 nm to reduce second harmonics from the monochromator and to prevent photons of lower wavelengths from reaching the sample. The ac beam is collimated using two lenses and focused down onto the sample between the probe contacts with a mirror. Since the lifetime of electron-hole pairs is constant, because of the dc light, the photocurrent corresponds directly to the absorption coefficient.

The optical absorption has an exponential energy dependence in the vicinity of the bandgap energy,

$$\alpha = \alpha_o \exp[-\frac{E_g - h\nu}{E_{ur}}]$$

where $(E_g\text{-}h\nu)$ is the photon energy, α is the absorption coefficient, E_{ur} is the Urbach energy. Since for low α, QE values are directly proportional to $(\alpha.t)$, plotting ln(QE) versus photon energy, we can obtain Urbach energy from the slope.

The slope is called the Urbach energy after the first observation of the exponential tail in alkali halide crystals by Urbach [32]. It is found in all amorphous semiconductors. The shape of the absorption edge is simply given by the joint density of states and so reflects the disorder broadening of the bands [3]. For low defect density a-Si:H the valence band tail has a slope of about 45 meV. It is broader than the conduction band tail and so dominates the joint density of states, and is indeed close to the Urbach energy. This explanation implies that excitonic effects are not significant since they are not described by the one particle density of states distribution. Since the Urbach energy reflects the shape of the valence band tails, it follows that the Urbach energy varies

(increases) with the structural disorder. There is a larger value of the Urbach energy for low bandgap a-Si:Ge alloys.

The exponential region is followed by an additional absorption band between localized defects (dangling bonds) and extended band states at lower photon energies. This gives rise the low energy shoulder seen in the spectra in Figure 3.5.

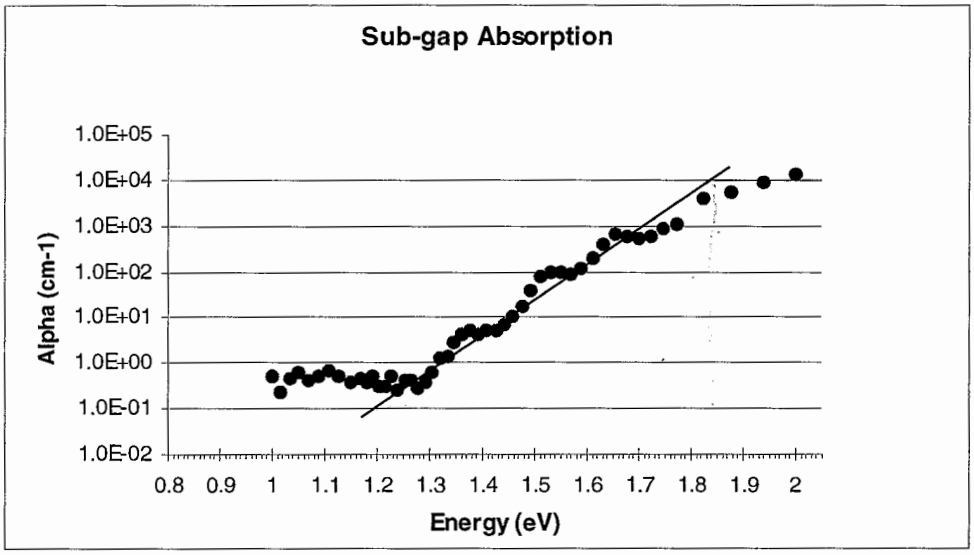

Figure 3.5 Plot showing sub-gap absorption. The slope of the linear part gives the Urbach energy of the material. The line is a guide to the eye

3.2 Characterization Of Devices

3.2.1 Thickness

Since devices are deposited on stainless steel substrate, reflection measurements are used to determine the thickness with the spectro-photometric technique. The thickness equation is the same as the one used for films.

3.2.2 I-V Characteristic

The performance of a p-i-n solar cell can be completely described by the current-voltage characteristic. The photocurrent rapidly saturates in reverse bias when there is full collection of the incident absorbed photon flux. The photovoltaic properties in

slightly forward bias are characterized by the short circuit current J_{sc}, the open circuit voltage, V_{oc}, and the fill factor, F (Figure 3.6). The maximum power delivered by the device is the product of the three terms

$$P_{max} = J_{sc} V_{oc} F$$

The J-V characteristic of the device is given by

$$J(V) = J_s \exp[\ (qV/AkT) - 1\ ] - J_L(V)$$

where J is the current at a voltage V, J_s the reverse saturation current, A the diode factor, T the temperature and J_L is the light generated current.

The parameter J_{sc} which is the short-circuit current is defined as the current of the cell under illumination for V=0, and is equal to J_L the photogenerated current. It depends on the incident spectrum, the response of the material and the collection efficiency.

$$J_L = q \int (1-R)\ Q(E)\ S(E)\ dE$$

where R is the reflection coefficient of the material, S(E) the photon flux of the incident solar spectrum and Q(E) the energy-dependent collection efficiency.

The open-circuit voltage V_{oc} is obtained for J(V) = 0. Since V_{oc} depends on the ratio J_L/J_S, it is determined by the absorption and light-generation process and the efficiency with which the charge carriers reach the depletion region. The open-circuit voltage is related to the built-in potential and the electrical quality of the junction as well. A typical a-Si:H built-in potential is of 1.2V. The open circuit voltage cannot exceed this value and as a rule is limited to about 80% of the maximum.

The fill factor, F provides a measure of the quality of the material used in the i-layer, and the cell design. While in a crystalline silicon solar cell F is largely determined by the contact resistance, in amorphous silicon the charge collection efficiency is more important. A high fill factor requires low loss of photogenerated carriers in the i-layer and at the interfaces, strong electric field in the i-layer, and a good ohmic contact.

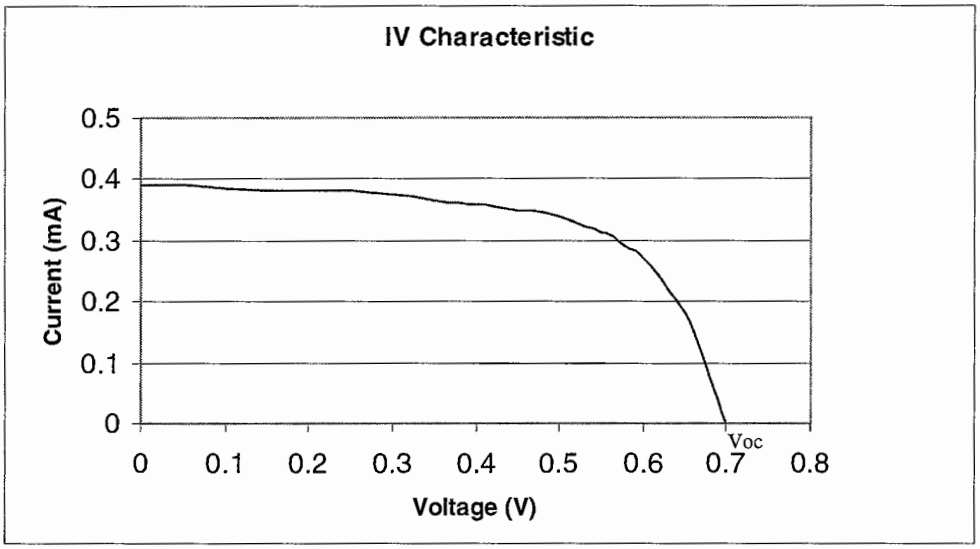

Figure 3.6 The IV characteristic of a good device. The fill factor is about 67%

Finally, the solar cell efficiency can be determined as

$$\eta = J_{sc} V_{oc} F / \phi_{in}$$

where ϕ_{in} is the incident solar power and is about 100mW/cm^2.

3.2.3 Quantum Efficiency

Quantum efficiency (QE) is defined as the ratio of the number of charge carriers collected to the number of photons incident on the sample at a particular wavelength. A plot of QE versus the incident wavelength (Figure 3.7) gives the spectral dependence of the charge collection. The collection efficiency peaks at about 80-90 % for wavelengths between 500-600 nm, indicating that there is little loss due to recombination. The reduction at long wavelengths is due to the decreasing absorption coefficient. In fact, low band gap alloys such as a-Si:Ge, extend the spectrum to lower energies than a-Si.

The decreasing collection efficiency at shorter wavelengths can be attributed to several reasons. One is the absorption of light in the p layer that is directly exposed to the

incident light. The resulting photo-excited carriers give little contribution to the charge collection because of the low minority carrier lifetime in the doped material.

The diffusion of carriers in the intrinsic layer against the internal field also reduces the collection efficiency. The effect of back diffusion is most significant at high photon energy when the absorption length is less than 100 nm and the charge collection is reduced at wavelengths below 500 nm. Devices operating at reverse bias are less susceptible because the internal field is larger. The back diffusion is further enhanced by hot carrier effects as at high photon energies, electron-hole pairs are created with excess energies and they rapidly diffuse 5-10 nm during thermalization to the band edges.

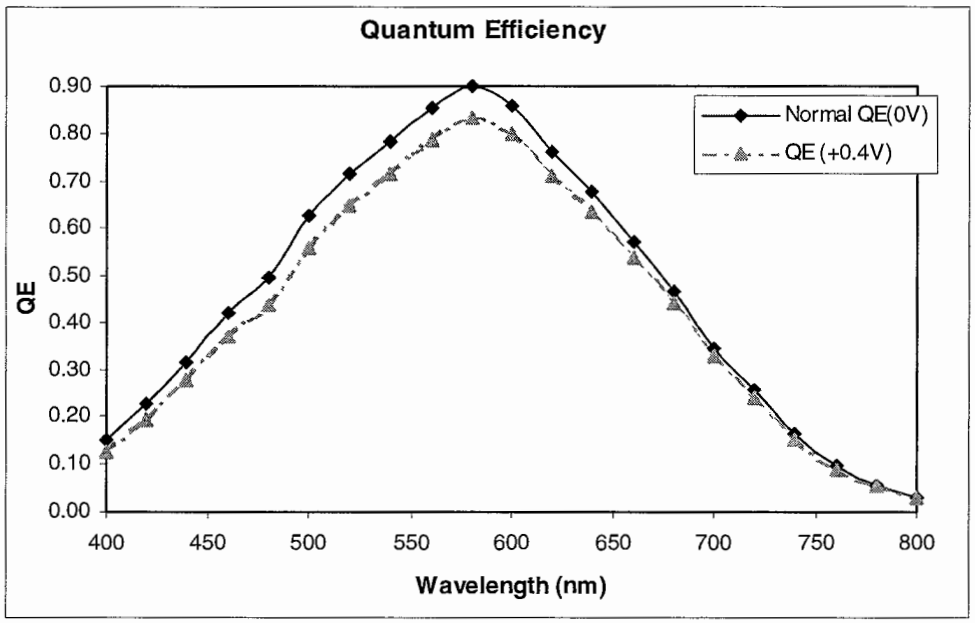

Figure 3.7 Plot showing the spectral dependence of the charge collection

The ratio of the QE values under zero and forward bias (Figure 3.8) provides a diagnostic tool [28]. A high ratio at lower wavelengths indicates a problem with the p-layer or p-i interface. When the bandgap of the buffer layer is too high, a notch develops [28,29] in the valence band between the buffer layer and the i-layer, leading to trapping of holes. This increases the QE ratio at short wavelengths. A larger ratio at large wavelengths is an indication that the holes being created are not being collected, and need a greater field assist. This indicates a poorer i-layer for the device.

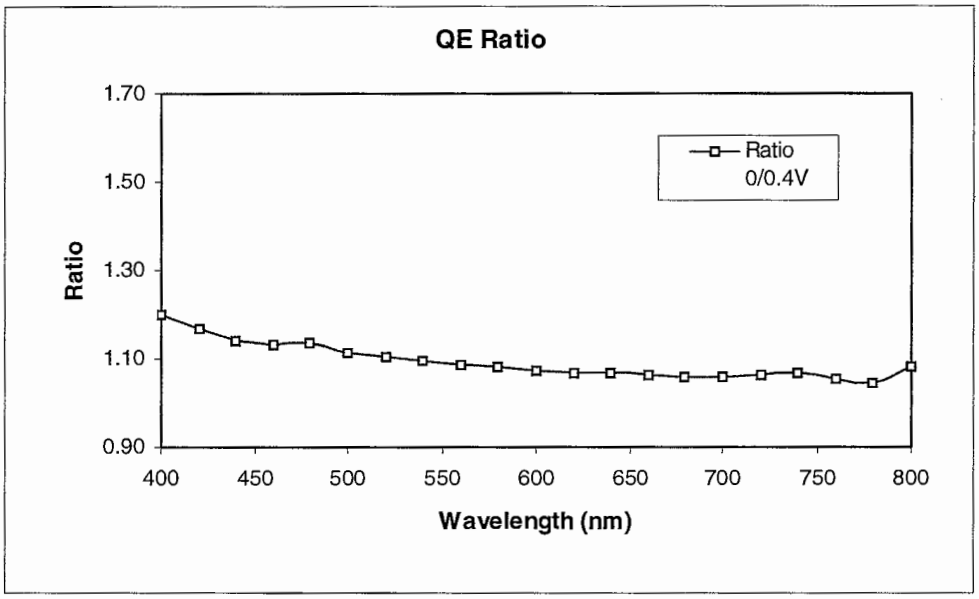

Figure 3.8 Plot showing the ratio of the QE values without and with a positive bias for the device in Figure 3.7

3.2.4 Urbach Energy and Mid-gap States

For the p-i-n devices, both types of defect, the tails states near the conduction and valence bands, and the mid-gap defect states play an important role in determining properties. The tail states limit the movement of level upon light excitation, limiting the open-circuit voltage of a solar cell. The mid-gap states provide an effective recombination mechanism for excess carriers thereby, reducing the diffusion length of minority carriers and limiting fill factors and open-circuit voltages of the cells. A high density of midgap states also reduces the electric field in the middle of the device which reduces the range of the minority carriers. The measurement of sub-gap quantum efficiency (QE) of the device at zero or reverse bias (Figure 3.9) is seen to provide an accurate picture of the Urbach energy of the i-layer of the device [28].

A solar cell is a minority carrier device with holes being the minority carriers. Therefore, the QE of a device for sub-gap photon energies is primarily a measure of the collection of holes generated in the bulk of the i-layer by the monochromatic beam incident on the cell. For photon energies near the bandgap, the photon beam is initially exciting the electrons from the valence band tails states into the conduction band. The

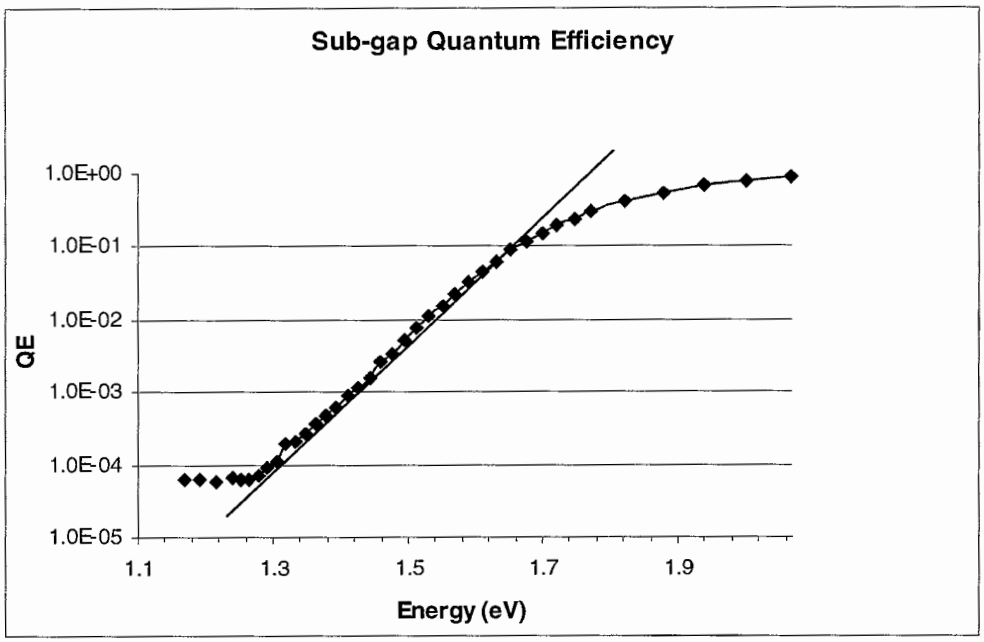

Figure 3.9 Plot of the sub-gap QE versus photon energy. The slope of the linear portion gives the Urbach energy for the material. The line is a guide to the eye

holes are generated near the valence band edge and are thus thermalized i.e. in contact witht the valence band as opposed to the holes generated in the mid-gap states. Thus the holes generated by the near bandgap photon energies will be easily collected, whereas the deep-lying holes generated by much smaller photon energies may get trapped and not collected. An external voltage helps to distinguish between the two types of holes, as shallow holes do not need significant field assist to be collected [28].

4. EXPERIMENTAL RESULTS

4.1 Properties Of Films

Films are grown at a microwave power of 150W in a He plasma (50sccm). The parameters varied are pressures of 15mT and 20mT; temperatures of 300C and 350C; and germane flow rates of 30%, 40% and 50% corresponding to approximately 5sccm, 7sccm and 8.5sccm respectively. The silane flow rate is kept at 15% or about 3sccm.

As expected and seen from Figures 4.1 and 4.2, the E04 energy and the Tauc energy decrease with increasing germane flow rates which indicates more germanium being incorporated in the film.

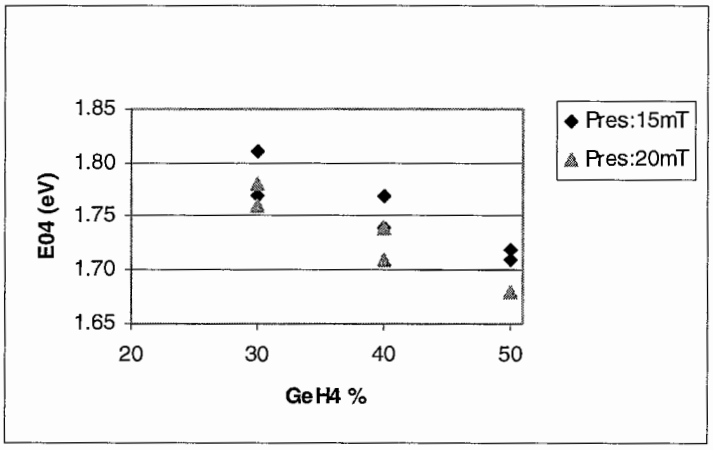

Figure 4.1 Variation of E04 energy with Germanium flow rate

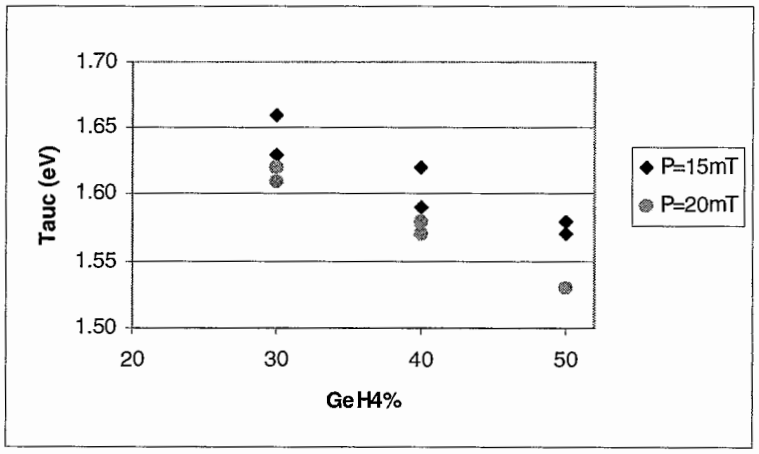

Figure 4.2 Variation of the Tauc energy with germanium flow rate

Also a possibly higher energy gap for films grown at 15mT compared to those at 20mT is noticed which indicates, probably lesser germanium is being incorporated. Figure 4.3 shows the absorption coefficient for two films grown at different pressures, 15mT and 20mT, keeping all other parameters including the silane/germane ratio, the same. These results compare well with those reported by Dalal et al earlier for slower growth rates of 1-2 A/sec [35].

Figures 4.4 shows the variation of the photosensitivity with the E04 energy at different pressures. It is seen that the photosensitivity decreases with a decrease in the

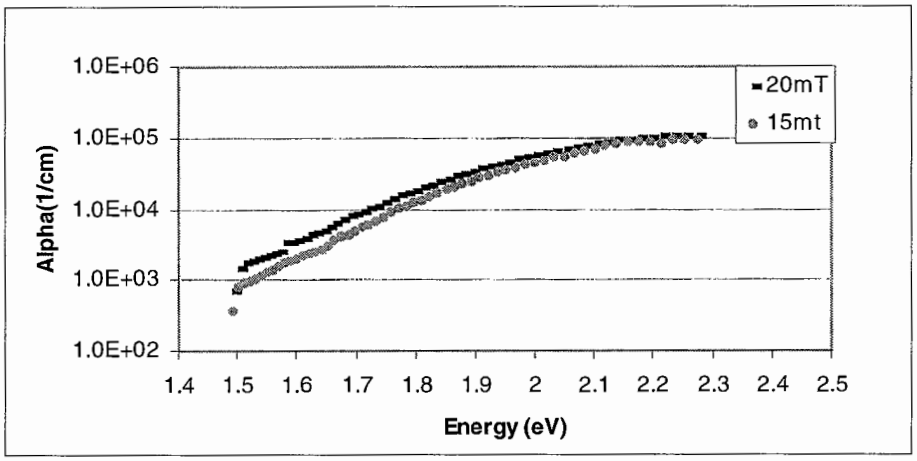

Figure 4.3 The Absorption Coefficient for two films grown at different pressures with the same silane/germane ratio

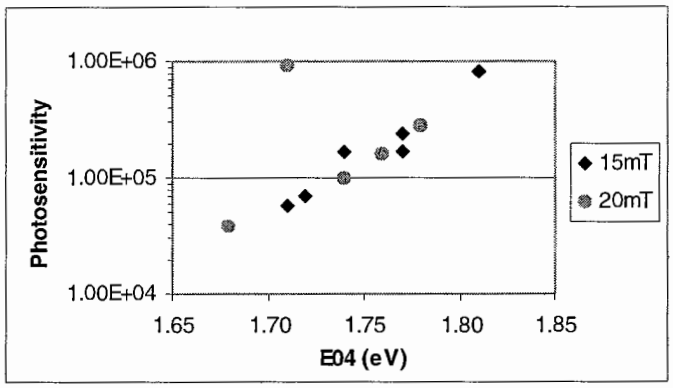

Figure 4.4 Photo/dark conductivity ratio as a function of the E04 energy for the films

band gap. This agrees with the trends reported in literature [15,16]. Figure 4.5 shows the mobility lifetime product for electrons as a function of the Tauc gap.

Figure 4.6 shows the Urbach energy of the films as a function of the optical bandgap. It is seen that Eur doesn't show any clear correlation with the bandgap. This agrees with the results from different deposition processes [16]. In our case, from figure 4.7, a lower Urbach energy is noticed for a germane flow of 40% (or about 7 sccm) and is used for the intrinsic layer of the p-i-n devices fabricated later.

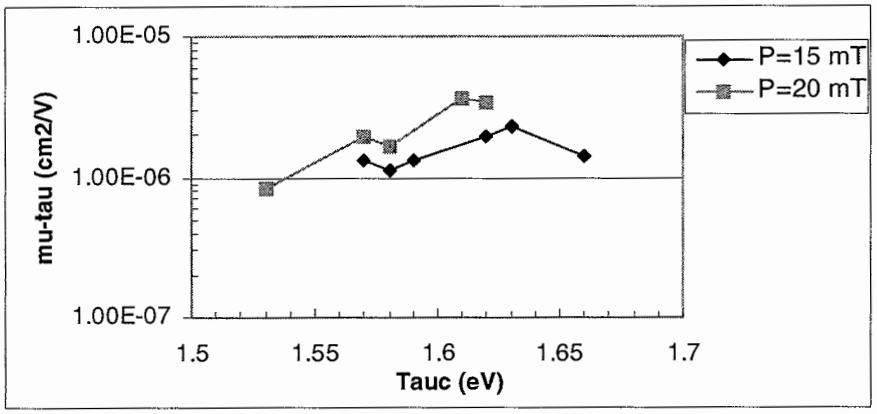

Figure 4.5 Variation of mobility-lifetime product for electrons with Tauc gap

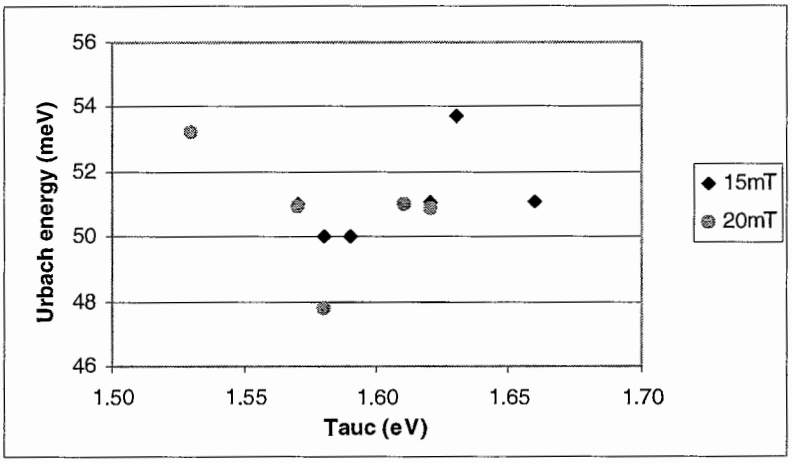

Figure 4.6 Variation of the Urbach energy with the Tauc optical bandgap. No clear correlation is noticed

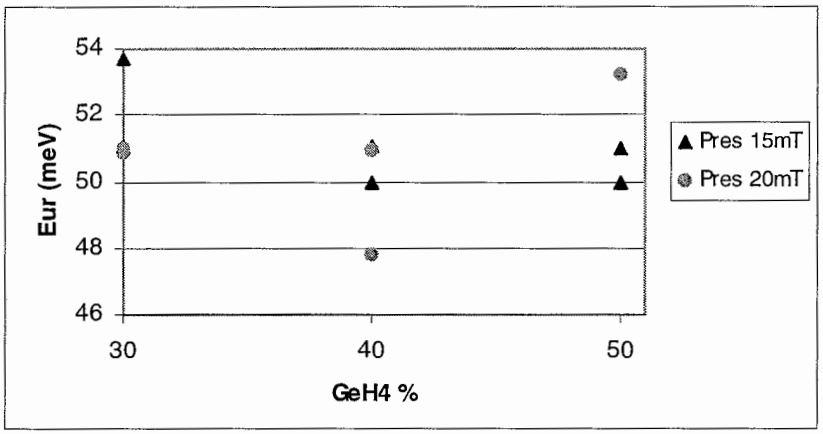

Figure 4.7 Variation of the Urbach energy with Germanium flow rate

4.2 Properties Of Devices

Based on the observation for the films, p-i-n devices were fabricated. The parameters for the i-layer were chosen from the film results with a temperature of 300C; microwave power of 150W; and a chamber pressure of 15mT. The plasma was He at 50sccm, and silane flow was at about 3sccm. The 10% germane flow rate was kept at 40% or about 7sccm; a few devices were also fabricated at 50% (~8.5sccm) germane flow.

In order to minimize the phosphorus contamination from the n to the i-layer, the later is compensated with boron, using hydrogen diluted trimethyl borane (TMB) as the compensating gas [14]. The device properties measured include the I-V characteristic, the QE and the Urbach energy of the valence band of the material. The fill factor and the voltage for the Al/Cr/p/i/n/ss devices are meaningful; the current because of absorption in the top Cr contact is not.

Figure 3.6 in the previous section shows the IV characteristic of a good device. We were able to achieve a fill factor of 67% for that device with open-circuit voltage of 0.69V and short-circuit current of 0.37mA.

The quantum efficiency of the devices under zero and small forward bias was measured. All devices had a maximum quantum efficiency of about 90% at around

580nm. Figure 4.8 shows the QE as a function of the incident photon wavelength for two devices.

We also tried adding 10% or 7sccm hydrogen to the plasma. Figures 4.9 and 4.10 show the effect of hydrogen for two different germane flow rates. In both cases,

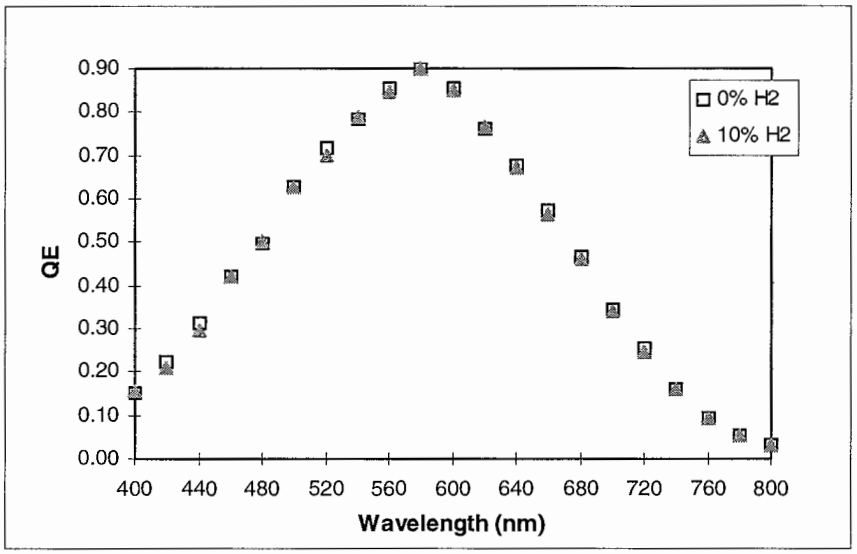

Figure 4.8 Quantum Efficiency versus wavelength for two cells. The one with 10% Hydrogen has the IV shown in Figure 3.6

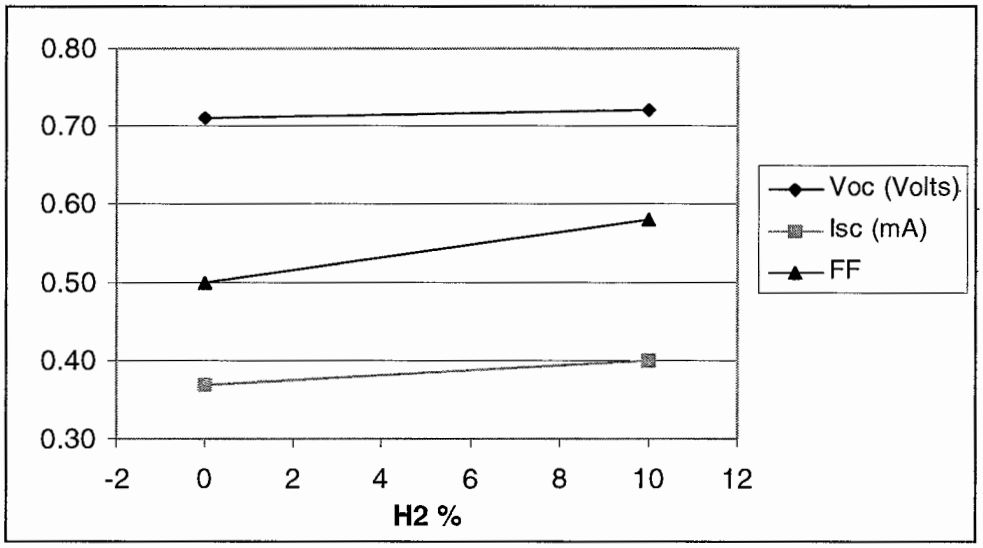

Figure 4.9 Effect of the presence of Hydrogen in the Plasma on device characteristics for Germane 40% flow

comparable or higher open-circuit voltage, short-circuit current and better fill factors are observed. The thicknesses of the devices were similar in each case.

One consequence of hydrogen in the plasma is the reduction in the growth rate. For example, the growth rates for the cells shown in Figure 4.8, the one with hydrogen

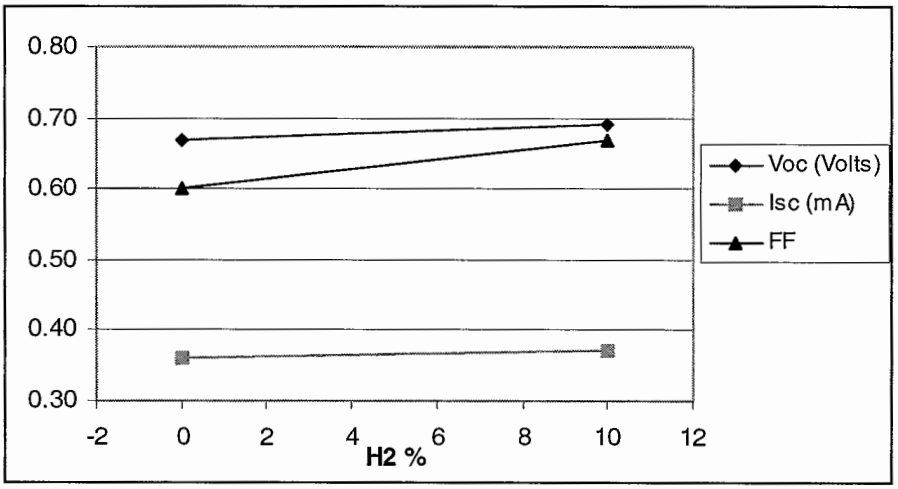

Figure 4.10 Effect of the presence of Hydrogen in the Plasma on device characteristics for Germane 50% flow

present had a rate of ~2.5 A/sec compared to ~3.5 A/sec for the one without hydrogen in the plasma. Figure 4.11 shows the subgap QE for the devices.

The Urbach energy of the i-layer material can be measured from the slope of the linear portion of the plot in Figure 4.11. As mentioned earlier, the Urbach energy gives an indication of material quality. We obtained Urbach energies in the range of 45-47 meV indicating good quality material.

Moreover, from Fig 4.11, hydrogen seems to cause a slight, though not significant, increase in the Tauc gap.

The effect of the SiC buffer layer between the p and i-layers is also sought to be observed. The conflicting requirements of a thicker buffer for better control of the band gap grading, and a thinner buffer to allow good hole transport are not always met. Three buffer layer growth times of 20x3, 30x3 and 45x3 seconds are investigated. Figure 4.12

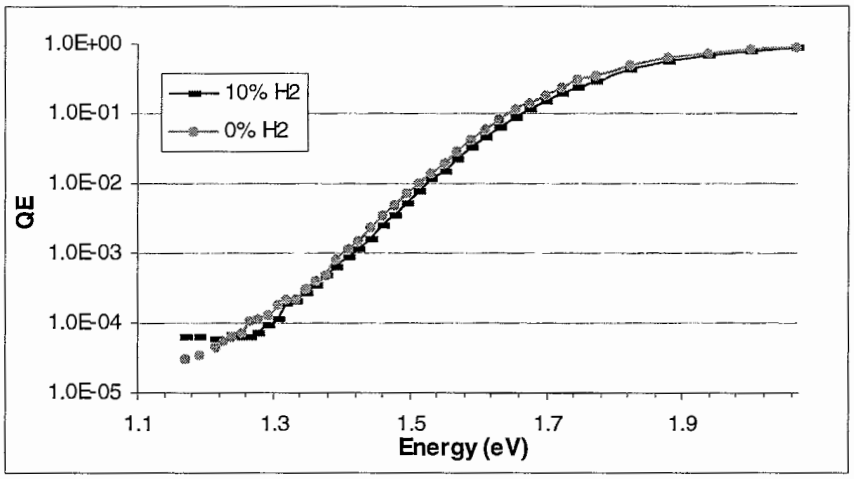

Figure 4.11 The sub-gap QE for the devices in Fig 4.8. The Urbach energy is ~47meV

shows the results. Its seen that a graded buffer layer growth time of 45sec each has the best device properties in terms of higher open-circuit voltage, short-circuit current, better fill factor and lower Urbach energy. The QE ratio of the device for the three growth times is shown in Figure 4.13.

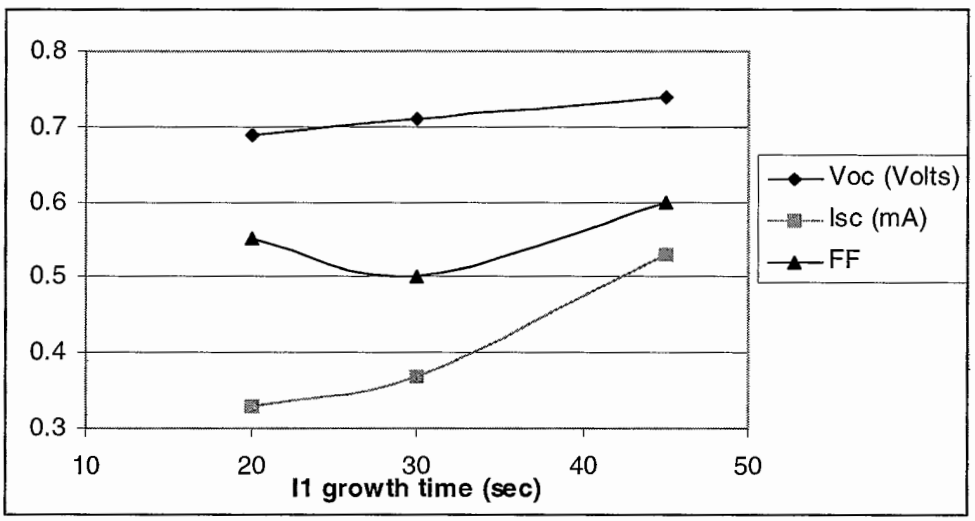

Figure 4.12 Effect of the buffer layer on the device characteristic

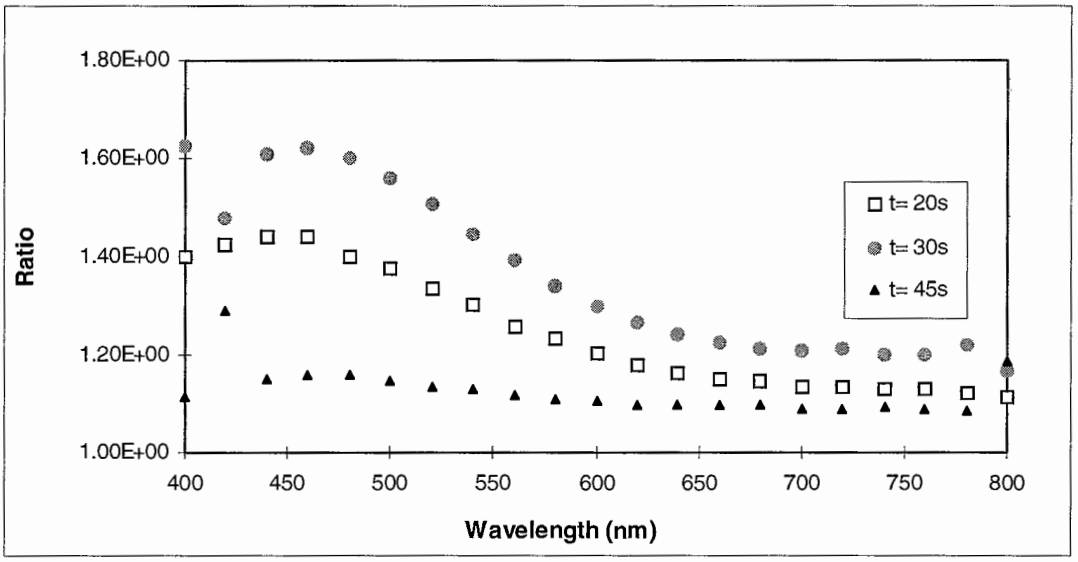

Figure 4.13 Effect of the buffer layer on the QE ratio 0/0.4 V

A buffer layer of 45 seconds seems to have the best properties in terms of a low QE ratio over the entire spectrum of interest. This indicates a good p-i interface as well as good carrier collection properties in the wavelength range investigated.

5. DISCUSSION AND CONCLUSION

Good quality a-SiGe:H films and p-i-n solar cells were fabricated at high growth rates using a He plasma. Since the number of films and devices that were fabricated are less, more samples are needed to verify the repeatability of the observations and results.

We had reasonable photosensitivity and Urbach energy values for the fabricated films. We obtained a photosensitivity of 3.9E4 and photoconductivity of ~3E-5 S/cm for sample with Tauc 1.55 eV. This value is better than or comparable to results for 1.5 eV optical gaps reported by Tsuo and Luft [4] for various deposition methods. Urbach energies for our films were slightly higher than those reported. It also seems that less Ge is incorporated at lower pressure as reported previously by Dalal et al [35].

We fabricated p-i-n solar cells using the optimum deposition parameters based on the film properties. The devices had graded ppm boron doping in the i-layer increasing in concentration from the n to the p layer. This helps to provide a slight field-assist to the holes. We achieved a Voc = 0.69V with a 67% fill factor with good QE properties and a low Urbach energy of 47 meV. It also seems that a SiC buffer layer grown for 45 seconds is better than 20 sec or 30 sec deposition times. A 45-second buffer seems to give more stable QE ratio indicating a device with good carrier collection. The low QE ratio (QE at 0V/0.4V) across the entire wavelength range is an indication that recombination is low at both the front p-i interface, and in the bulk of the device for a buffer layer grown for 45 seconds. Also a 10 % H2 - 100 % He plasma seems to give better results.

It is believed [17,18] that helium dilution effects are due to the enhanced bombardment of the film surface by helium ions during growth. This also can explain the seemingly lesser Ge incorporation at lower pressure. Film growth on the substrate involves surface diffusion of deposition radicals and hydrogen elimination.. It is possible that the surface mobility of the heavier, and therefore less diffusing, germyl radical on the growing film surface is enhanced by helium ion bombardment. This would lead to fewer Ge-Ge clusters and a more homogeneous structure with better properties and higher band gap.

The presence of hydrogen in the helium plasma seems to be beneficial because we achieve both the useful etching effects of hydrogen as well as effective momentum transfer to the radicals. Presence of hydrogen in the plasma reduced the growth rate, probably because of etching of the growing film by hydrogen. The beneficial effect of hydrogen in various applications is offset by the decrease in the deposition rate.

In conclusion, we feel it is possible to fabricate good quality a-SiGe films and devices at high growth rates (~ 5 A/sec) using a He plasma in an ECR-CVD system. Further studies on the reproducibility of the results and the possibility of increasing the growth rates more needs to be done. Also films with lower (<1.5eV) Tauc bandgaps need to be investigated.

APPENDIX

Figure A.1 A Schematic of the ECR-CVD System used for Fabricating the Samples:

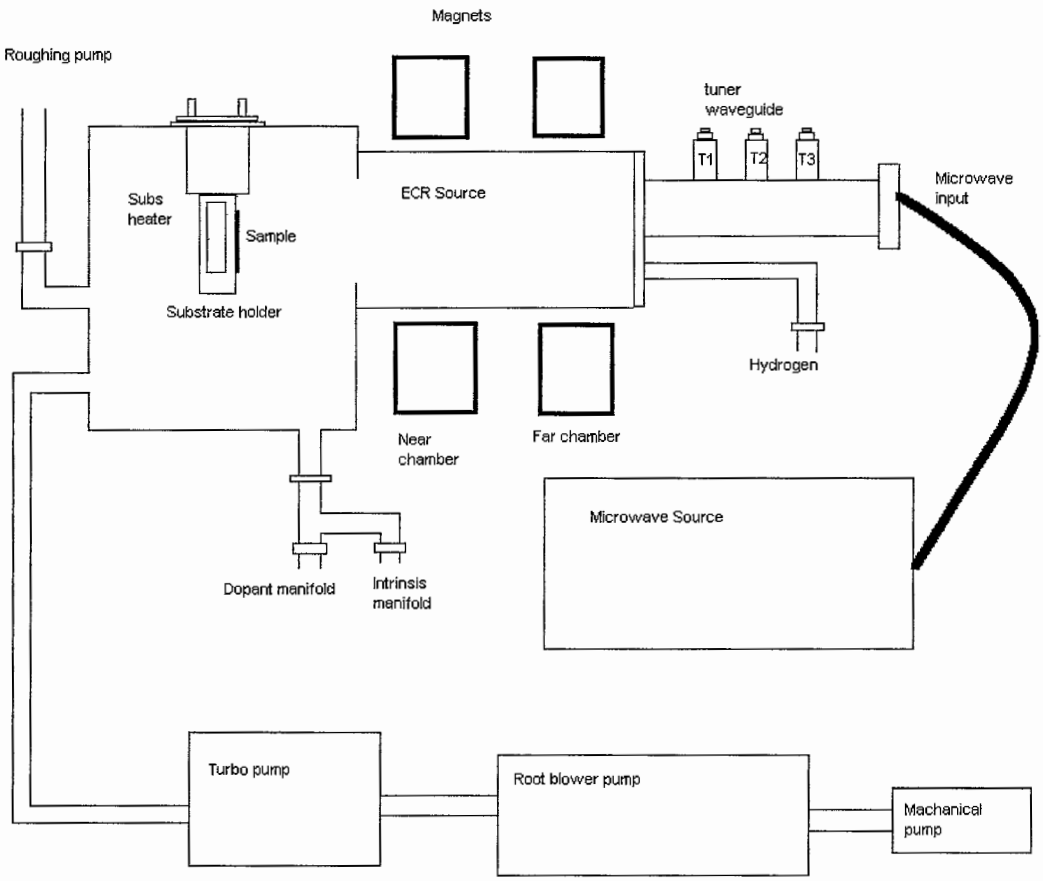

Figure A.2 A Schematic showing the Activation Energy Measurement Setup:

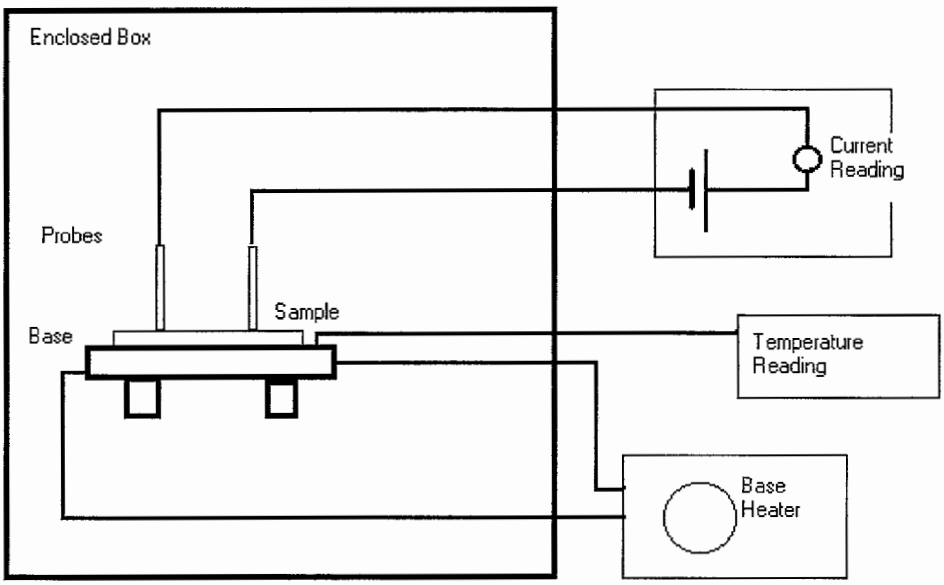

Figure A.3 A Schematic of the Apparatus used for the Two-Beam Photoconductivity Setup used for Sub-gap Absorption, and Quantum Efficiency Measurements:

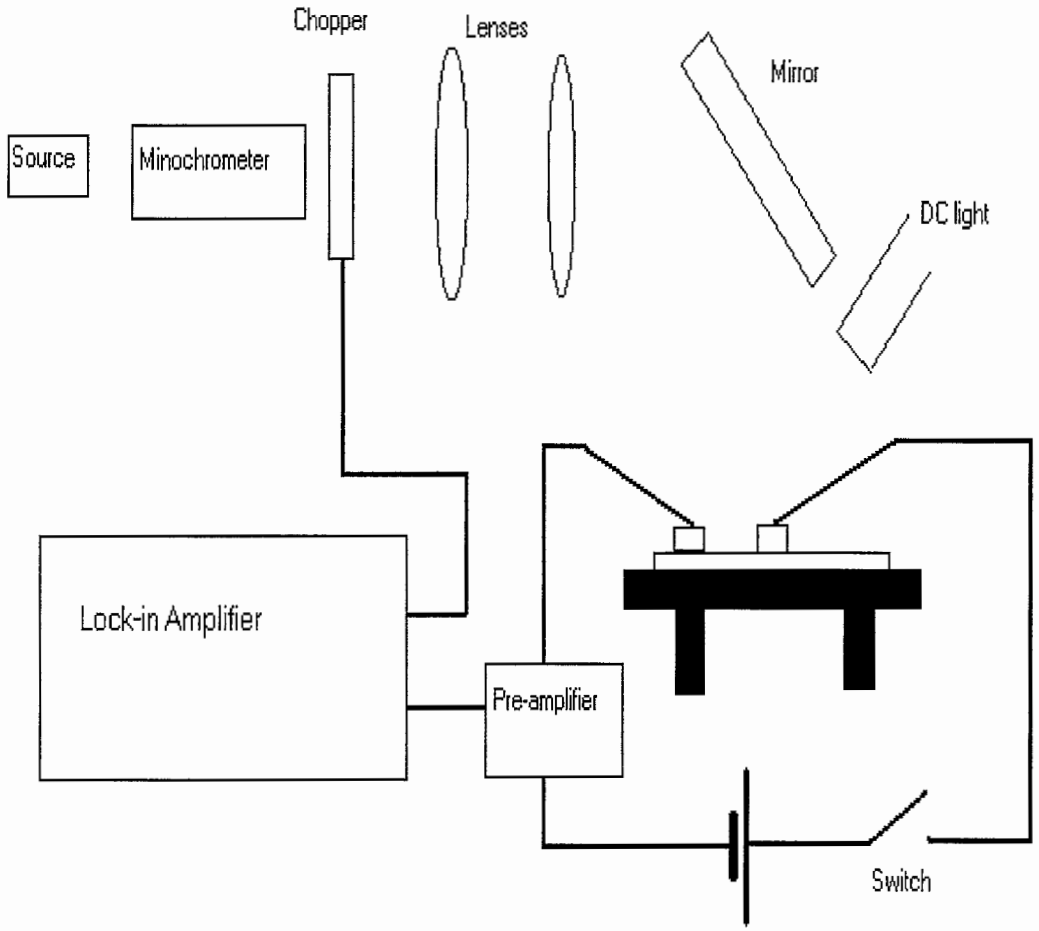

REFERENCES

1. Carlson, D.E., Wronski, C.R. (1976) "Amorphous silicon solar cell" *Appl Phys Lett* **28**, 671.

2. Madan, A., Shaw, M.P. (1988) *The Physics and Applications of Amorphous Semiconductor*, Academic Press, San Diego.

3. Street, R.A. (1991) *Hydrogenated Amorphous Silicon*, Cambridge University Press, Cambridge.

4. Chevallier, D., Wieder, H., Onton, A., Guarnieri, C.R. (1977) "Optical properties of amorphous $Si_xGe_{1-x}(H)$ alloys prepared by RF glow discharge" *Solid St Comm* **24**, 867.

5. Yang, J., Banerjee, A., Guha, S. (1997) "Triple-junction amorphous silicon alloy based solar cell with 14.6% initial and 13.0% stable conversion efficiencies" *Appl Phys Lett* **70**, 2975.

6. Stiebig, H., Ulrichs, S., Kulessa, T., Folsch, J. (1996) "Transient photocurrent response of a-Si:H based three color nipin detector" *J Non-Cryst Sol* **198-200**, 1185.

7. Tsuo, Y.S., Luft, W. (1990) "Alternative deposition processes for hydrogenated amorphous silicon and related alloys" *Appl Phys Comm* **10**, 71.

8. Doyle, J.R., Doughty, D.A., Gallagher, A. (1992) "Plasma chemistry in silane/germane and disilane/germane mixtures" *J Appl Phys* **71**, 4727.

9. Dalal, V.L., Kaushal, S., Xu, J., Han, K. (1994) "A critical review of the growth and properties of a-(SiGe):H" *Proc 24th IEEE Photovolt Spec Conf*, 464.

10. Matsuda, A., Ganguly, G. (1995) "Improvement of hydrogenated amorphous SiGe alloys using low power disilane-germane discharges without hydrogen dilution" *Appl Phys Lett* **67**, 1274.

11. Matsuda, A., Koyama, M., Ikuchi, N., Imanishi, Y. (1986) "Guiding principle in the preparation of high photosensitive hydrogenated amorphous SiGe alloys from glow discharge plasma" *Jpn J Appl Phys* **25**, L54.

12. Nozawa, K., Yamaguchi, Y., Hanna, J., Shimizu, I. (1983) "Preparation of photoconductive a-SiGe alloy by glow discharge" *J Non-Cryst Sol* **59-60**, 533.

13. Xu, X., Yang, J., Guha, S. (1996) "Hydrogen dilution effects on a-Si:H and a-SiGe:H material properties and solar cell performance" *J Non-Cryst Sol* **198-200**, 1113.

14. Sugiyama, S., Yang, J., Guha, S., Xu, X. (1996) "Light induced degradation of a-SiGe alloy solar cells deposited at high rates" *Mat Res Soc Symp Proc* **420**, 197.

15. Haku, H. (1991) "Preparation of a-Si and a-Si alloy films using an ion gun chemical vapour deposition method" *Jpn J Appl Phys* **30**, 1354.

16. Wickboldt, P. (1997) "High performance glow discharge a- $Si_{1-x}Ge_x$:H of large x" *J Appl Phys* **81**, 6252.

17. Middya, A.R., Ray, S. (1994) "Influence of deposition rate and hydrogen/helium dilution on the structural relaxation of a-SiGe:H network prepared at low substrate temperature" *J Appl Phys* **75**, 7340.

18. Middya, A.R., Ray, S., De, S.C. (1993) "Improvement in the properties of a-SiGe:H films: Roles of deposition rate and hydrogen dilution" *J Appl Phys* **73**, 4622.

19. Ikeda, T., Ganguly, G., Matsuda, A. (1996) "Factors limiting improvement of a-SiGe:H" *Proc 25th IEEE Photovolt Spec Conf*, 1157.

20. Guha, S., Xu, X., Yang, J., Banerjee, A.(1995) "Microwave glow-discharge deposition of amorphous silicon based alloys at high deposition rates for solar cell application" *Mat Res Soc Symp Proc* **377**, 621.

21. Saito, K., Sano, M., Ogawa, K., Kajita, I. (1993) "High efficiency a-Si:H alloy cell deposited at high deposition rate" *J Non-Cryst Sol* **164-166**, 689.

22. Sadamoto, M. (1996) "Improvement of the quality of a-SiGe:H film" *J Non-Cryst Sol* **198-200**, 1105.

23. Kutznetsov, V.I., Zeman, M., Girwar, B.S., Metselaar, J.W. (1996) " Electrical and optical properties of plasma deposited a-SiGe:H alloys: role of growth temperature and post-growth anneal" *J Appl Phys* **80**, 6496.

24. Terakawa, A., Shima, M., Sayama, K., Tarui, H. (1995) "Optimization of a-SiGe:H alloy composition for stable solar cells" *Jpn J Appl Phys* **34**, 1741.

25. Stutzmann, M., Street, R.A., Tsai, C.C., Boyce, J.B., Ready, S.E. (1989) "Structural, optical and spin properties of hydrogenated amorphous silicon-germanium alloys" *J Appl Phys* **66**, 569.

26. Tsuo, Y.S., Xu, X., Balberg, I., Crandall, R.S. (1991) "Effects of helium dilution on glow discharge depositions of a-SiGe:H alloys" *Proc 22nd IEEE Photovolt Spec Conf*, 1334.

27. Kaushal, S.K., Dalal, V., Xu, J. (1996) "Growth of high quality silicon-germanium films using low pressure remote ECR discharge" *J Non-Cryst Sol* **198-200**, 563.

28. Kaushal, S.K. (1997) "Stability and electronic properties of amorphous silicon p-i-n devices fabricated using ECR plasma enhanced chemical deposition" *PhD thesis, Iowa State University.*

29. Baldwin, G., Dalal, V., Han, K. (1993) "Deposition of high quality a-(Si,Ge):H films and novel graded gap devices using RF triode glow discharge deposition" *Proc 23rd IEEE Photovolt Spec Conf*, 1037.

30. Tauc, J., Grigorovici, R., Vancu, A. (1966) "Optical properties and electronic structure of amorphous germanium" *Phys Status Solidi* **15**, 627.

31. Lee, S., Kumar, S., Wronski, C.R. (1989) "A critical investigation of a-Si:H photoconductivity generated by subgap absorption of light" *J Non-Cryst Sol* **114**, 316.

32. Urbach, F. (1953) "The long wavelength edge of photographic sensitivity and of the electronic absorption of solids" *Phys Rev* **92**, 1324.

33. Luft, W., Tsuo, Y.S. (1993) *Hydrogenated Amorphous Silicon Alloy Deposition Processes*, Marcel Dekker, Inc., New York.

34. Finger, F., Beyer, W. (1998) "Growth of a-SiGe:H alloys by PECVD - optimization of growth parameters, growth rates, microstructure and material quality" *Properties of Amorphous Silicon and its Alloys*, INSPEC, United Kingdom.

35. Dalal, V., Maxson, T., Haroon, S. (1998) "Influence of plasma chemistry on the properties of amorphous (Si,Ge) alloy devices" *Mat Res Soc Symp Proc* **507**, 441.

ACKNOWLEDGEMENTS

I would like to take this opportunity to thank the various persons who have helped me during my research.

At the outset, my sincere gratitude goes out to my major professor Dr Vikram Dalal for his guidance and support in my graduate school years. Thanks are also due to Dr Gary Tuttle and Dr David Lynch for serving on my committee.

Thanks to Tim Maxson, Keqin Han, Zhiyang Zhou, Vu Anh Vu and Yong Liu for help with the samples. Thanks are also due to everybody in Dr Dalal's group and at MRC for their friendship and helping me get oriented. Thanks also go out to all my friends on campus, for their friendship, interesting discussions and making me feel at home in Ames. I am also thankful to Burha, Poali, Topu and my friends in India for their support and friendship.

Finally, I am grateful to my parents, my brother, Caushiq and the other members of my family without whose love, support and inspiration this would not have been possible.